Imperial College London

The Kosterlitz-Thouless Phase Transition in Spin Models and Quantum Field Theory.

Author:

Méabh Allen

Supervisor:

Arttu Rajantie

Submitted in partial fulfilment of the requirements for the degree of Master of Science of Imperial College London.

Department of Physics

October 1, 2021

Contents

List of Figures

Figure 1: Contour plot of the XY model showing presence of vortices and antivortices [1].

1 Introduction

The Kosterlitz–Thouless phase transition has garnered significant attention in the physics community in the last decade. A phase transition of the two-dimensional XY model in statistical physics, it is widely known for earning its namesakes the 2016 Nobel Prize 'for theoretical discoveries of topological phase transitions and topological phases of matter'.

Topological phase transitions are of fundamental interest due to their exotic nature. They occur at the boundary between a symmetric and broken phase of a physical system but are considered a separate class of phase transition. Topological phase transitions are special because they are distinct from the phenomenon of spontaneous symmetry breaking. Many aspects of topological physics are not fully understood and their obscure nature makes them difficult to study. KT transitions can be found in several two dimensional systems in condensed matter physics that are approximated by the XY model. More recently the term has been adopted by the superconductor community due to its link to vortices. Therefore developing numerical methods and establishing links with other branches of physics is of great interest to the current scientific community.

One premise of this project was to gain an understanding of the unique topological behaviour of the Kosterlitz-Thouless Phase Transition in the XY model. An accurate model of the system needed to be developed in order to do this. Monte Carlo computational methods

were used to simulate the behaviour of spins in finite square lattice volumes and physical observables were calculated to compare with current literature. Next, a comparison of XY and Ising model systems was carried out to show the distinct phase transition behaviour for discrete and continuous symmetries in low dimensions. A key question we then wanted to answer was whether or not a path integral action derived from a general O(n)-symmetric quantum field theory could be used to accurately describe such a classical spin system. The Monte Carlo model was adapted to this quantum path integral approach to verify if the field model would yield analagous results. With this achieved, a clear link was established between the underlying mathematics of classical spin physics and quantum theory.

Chapter 2 is devoted to the theoretical background necessary for this report. A brief overview of the statistical systems in question - the XY model and to an extent the Ising model - is presented and the relevant symmetries of the systems are discussed, specifically the distinction between the Kosterlitz-Thouless Phase Transition and Spontaneous Symmetry Breaking. The path integral method of Quantum Field Theory is presented and its relationship to the physical spin systems is outlined. Lastly, some important computational concepts are explained. In chapter 3 the numerical procedure developed to facilitate the project is examined in detail. The methods used to determine a spin configuration of N x N dimensions and its resulting range of physical observables is explained, as well as its error analysis. The adaptation of the algorithm to the O(n) field model is then outlined. In chapter 4, estimates for some physical observables of the xy system, such as energy, magnetism, heat capacity and susceptibility are presented for various lattice volumes. These results are examined in detail to outline the behaviour of the system in its symmetric, broken and critical temperature regimes. The results are compared to analagous Ising model estimates to distinguish the types of phase transition. Field theory results are presented. Chapter 5 suggests possibilities for future research. In chapter 6 conclusions are made regarding the results of the project.

2 Background Theory

2.1 Statistical Physics

2.1.1 The XY Model in Two Dimensions

The XY model is a classical statistical theory describing the spin configuration of atoms in a two-dimensional square lattice. Neighbouring spins $\vec{s}_i$ and $\vec{s}_j$ interact with each other. The Hamiltonian for such a two-dimensional system without an external magnetic field is

$$H = -J \sum_{\langle l,k \rangle} \vec{s}_l \cdot \vec{s}_k \tag{1}$$

where J represents the translation-invariant interaction that is set to 0 for non-nearest neighbours and where the spins have equal unit length

$$\vec{s}_i \cdot \vec{s}_i = 1 \tag{2}$$

Such a two dimensional spin can be described by an angle θ_i,

$$\vec{s}_i = \begin{pmatrix} \cos \theta_i \\ \sin \theta_i \end{pmatrix} \tag{3}$$

Leading to an O(2)-symmetric Hamiltonian

$$H = -J \sum_{<i,j>} \cos{(\theta i - \theta j)} \tag{4}$$

3
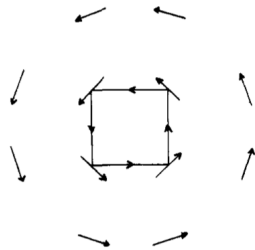
Figure 2: Closed loops around a single vortex [2].

It can be assumed that spin angles change sufficiently slowly from site to site in a real physical configuration and we can approximate the Hamiltonian using the Taylor expansion,

$$\cos(\theta i - \theta j) = 1 + \frac{1}{2}(\theta i - \theta j)^2 + \mathcal{O}(\theta i - \theta j)^4) \tag{5}$$

$$\approx 1 - \frac{1}{2}(\theta_i - \theta_j)^2 \tag{6}$$

In the continuum limit of this system, using the partial derivative $\theta_i - \theta_j = \partial_x \theta$, the Hamiltonian becomes

$$H = E_0 + \frac{J}{2} \int d\mathbf{r} (\nabla \theta)^2 \tag{7}$$

where E_0 is the ground state of aligned spins and $\nabla \theta$ is the Laplace operator [9].

We are interested in finding field configurations that correspond to local minima of H, that is

$$\frac{\delta H}{\delta \theta(\mathbf{r})} = 0 \Rightarrow \nabla^2 \theta(\mathbf{r}) = 0 \tag{8}$$

There are two possible solutions to this equation. The first solution just describes the ground state of the system,

$$\theta(\mathbf{r}) = const. \tag{9}$$

A more subtle but profound mathematical solution posits the existence of topological defects called vortices. An overview of some key complex analysis concepts is essential for understanding the unusual nature of these topological vortices.

4

The Cauchy Residue Theorem is a useful tool for evaluating line integrals of analytic functions over closed curves in the complex plane and can be adapted to the real plane. Consider a function $f(z)$ that is holomorphic (one that is locally complex-differentiable) at all but a finite number of singularities z_k on a simply connected open subset U of the complex z-plane. The Cauchy Residue Theorem then states that the line integral of such a function along a closed loop is determined by the sum of the residues of singularities contained within the loop,

$$\oint f(z)dz = 2\pi i \sum_{k=1}^{n} \text{Res}\,(z_k) \tag{10}$$

Here z_k are singularities of the function f, i.e, points in the z-plane where $f(z_k)$ is non-analytic.

Adapting to this to the case of the real-plane, let us denote the contribution of the "residue" of a single vortex of strength n such that the closed loop

$$\oint \nabla\theta(\mathbf{r}) \cdot d\mathbf{l} = \begin{cases} 2\pi, & \text{vortex enclosed} \\ \\ 0, & \text{otherwise} \end{cases} \tag{11}$$

The system is spherically symmetric, i.e., $\theta(\mathbf{r}) = \theta(r)$, so the solution for the line integral is calculated simply as

$$\oint \nabla\theta(\mathbf{r}) \cdot d\mathbf{l} = 2\pi r |\nabla\theta| \tag{12}$$

and an expression for the Laplace operator can be obtained,

$$|\nabla\theta(r)| = \frac{n}{r} \tag{13}$$
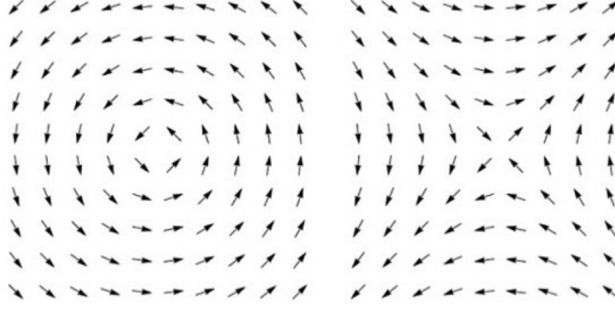
Figure 3: Vortex-anti-vortex pair with 2π and -2π loop contributions.

The energy of a n-charged vortex can then be determined,

$$E_{vor} - E_0 = \frac{J}{2} \int d\mathbf{r} [\nabla \theta(\mathbf{r})]^2 \tag{14}$$

$$= \frac{Jn^2}{2} \int_0^{2\pi} \int_a^L r dr \frac{1}{r^2} \tag{15}$$

$$= \pi J n^2 \ln\left(\frac{L}{a}\right). \tag{16}$$

This circulation condition creates a distortion in the phase field that persists infinitely far from the centre of the vortex. The vortex energy scales quadratically with the vortex strength and so the effect of a single vortex is considerable. The free energy of a single vortex is

$$F_{vor} = E - TS \tag{17}$$

$$= E_0 + (\pi J - 2k_B T) ln(\frac{L}{a}) \tag{18}$$

where $S = k_B ln(\frac{L^2}{a^2})$ is the entropy of the system, L is the system size and a is the vortex size. Clearly then

$$\lim_{L \to \infty} F_{vor} \to \begin{cases} \infty, & \text{for } T < \frac{\pi J}{2k_B} \\ -\infty, & \text{for } T > \frac{\pi J}{2k_B} \end{cases} \tag{19}$$

so vortex and anti-vortex pairs only proliferate above certain temperatures to prevent energy divergence. At low temperatures they are bound together but above a critical temperature

6

they unbind and impose a topological order on the system. The thermodynamics of the system can then be described using the partition function

$$Z = e^{-\beta E_0} \int D[\theta] \exp\left\{-\beta \frac{J}{2} \int d\mathbf{r}(\nabla\theta)^2\right\} \tag{20}$$

Taking a closer look at the spin-spin correlation function in the low temperature regime and therefore ignoring vortex contributions,

$$\langle \boldsymbol{S}_i \cdot \boldsymbol{S}_j \rangle = \langle \exp\left\{i\left(\theta_i - \theta_j\right)\right\}\rangle = \exp\left(-\frac{k_\mathrm{B}T}{2J}g\left(r_i - r_j\right)\right) \tag{21}$$

where it can be shown that [11],

$$g(r) \approx 2\pi \ln\left|\frac{r}{r_0}\right| \tag{22}$$

We find that the correlation function follows a power law,

$$\langle \boldsymbol{S}_i \cdot \boldsymbol{S}_j \rangle \propto \left|\frac{\boldsymbol{r}_i - \boldsymbol{r}_j}{r_0}\right|^{-k_\mathrm{B}T/4\pi J} \tag{23}$$

In the Kosterlitz Thouless phase, when the contribution of vortices is taken into account,

$$\langle \boldsymbol{S}_i . \boldsymbol{S}_j \rangle = \langle \exp\left\{i\left(\theta_i - \theta_j\right)\right\}\rangle \langle \exp\left\{i\left(\bar{\phi}_i - \bar{\phi}_j\right)\right\}\rangle \tag{24}$$

the correlation function is found to follow an exponential decay,

$$\langle \boldsymbol{S}_i \cdot \boldsymbol{S}_j \rangle \propto \exp^{-\frac{r}{\xi}} \tag{25}$$

Thus there is a distinct difference in the spin-spin correlation behaviour in the symmetric and Kosterlitz-Thouless phases of the system.
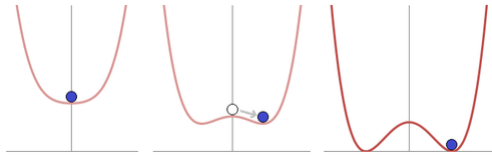
Figure 4: Spontaneous symmetry breaking for a single-component classic scalar field.

2.1.2 Symmetry Breaking & Phase Transitions

This vortex-antivortex binding-unbinding indicates the existence of a phase transition at a finite critical temperature. The Mermin Wagner Theorem states that continuous symmetries cannot be spontaneously broken at finite temperature in systems with sufficiently short-range interactions in dimensions $d \leq 2$ [7]. The XY model has a continuous rotational symmetry and so should not exhibit any long-range order. The subtlety of this phase transition is that it is topological in nature and does not violate the theorem. Certain correlations become algebraic below the critical temperature in a Kosterlitz Thouless phase that is distinct from spontaneous symmetry breaking. Let us take a closer look at what we mean by spontaneous symmetry breaking. The Lagrangian of a single-component real scalar field ϕ is given by [?]

$$\mathcal{L} = \frac{1}{2}\partial_\mu\phi\partial^\mu\phi - V(\phi) \tag{26}$$

where $V(\phi)$ is the potential,

$$V(\phi) = \frac{1}{2}m^2\phi^2 + \frac{1}{4}\lambda\phi^4 \tag{27}$$

For $m, \lambda > 0$, the ground state of the potential occurs at a unique vacuum state $\phi = 0$. If $m^2 = -\mu^2$ however, deviations from this vacuum state can be achieved: though the Lagrangian of a field theory is invariant, the state needn't be. We are interested in determining the minimum of the potential, the vacuum state ϕ_0, such that

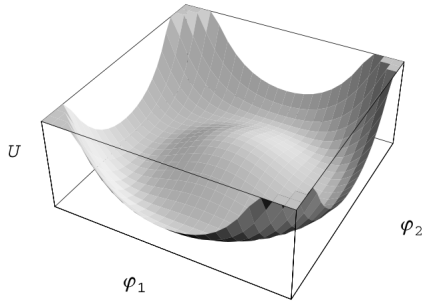$$\frac{\partial V(\phi)}{\partial \phi}\bigg|_{\phi_0} = 0 \tag{28}$$

Figure 5: "Mexican hat" shape of the potential V for $\mu^2 > 0$[?] in a two-component scalar field theory, analagous to the two-dimensional Ising Model.

which yields symmetric solutions of the form as shown in Figure 4

$$\phi_0 = \begin{cases} \pm\sqrt{\frac{2\mu^2}{\lambda}}, & \text{minima} \\ \\ 0, & \text{maximum} \end{cases} \tag{29}$$

This single field theory can be adapted to higher component fields and spacetime dimensions. In the case of two dimensions, as seen in Figure 6, the ground state is in fact infinitely degenerate and leads to the emission of massless Goldstone bosons.

2.1.3   The Ising Model in Two Dimensions

The Ising Model is a well-known example of a statistical spin system that contrarily does exhibit spontaneous symmetry breaking. The symmetry of the Hamiltonian,

$$H = -J \sum_{\langle l,k \rangle} s_l \cdot s_k \tag{30}$$

where the spins $s_i = \pm 1$, is a discrete rather than a continuous symmetry and so does not violate the Mermin-Wagner theorem [10]. The system is thus not explicitly forbidden from producing a massive particle and the vacuum expectation value of the system should accordingly tend to a non-zero constant. To support the distinction between the two-dimensional
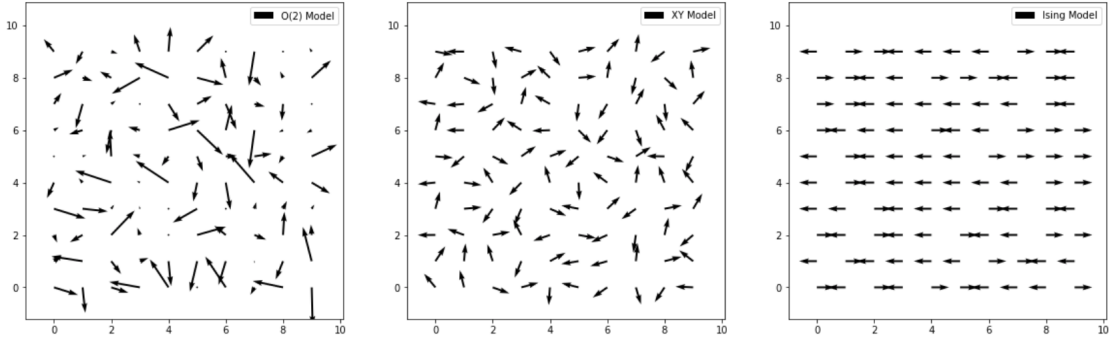
9

Figure 6: Comparison of the various spin models investigated in this project for a 10 x 10 lattice configuration. The O(2) model has two continuous symmetries, the XY model has one continuous symmetry and the Ising model has one discrete symmetry.

Ising and XY models, simulations for both were carried out for lattice sizes N = 20,40. The true value of the vacuum expectation value cannot be explicitly calculated in a finite volume, but comparing various lattice sizes can highlight the limit of such a constant. Such computations should support the distinction between the spontaneous symmetry breaking nature of the Ising model and the Kosterlitz Thouless phase transition of the XY model.

2.2 Quantum Field Theory

Spin systems can be considered from the point of view of quantum field theory. The discretised path integral approach of quantum field theories and statistical ensemble approximation methods are two sides of the same mathematical coin and can be shown to converge to be equivalent in the case of the XY model. The action of a O(n)-symmetric n-component field theory is [5]

$$S = -\int d^d x \left[\frac{1}{2} \partial_\mu \varphi^\alpha \partial_\mu \varphi^\alpha + \frac{1}{2} \mu^2 \varphi^\alpha \varphi^\alpha + \frac{1}{4} \lambda \left(\varphi^\alpha \varphi^\alpha \right)^2 \right] \tag{31}$$

where the case of n=4 describes the Standard Model in d=4 spacetime. Discretising the action path integral [?],

$$S = -\sum_x \left[\frac{1}{2} \partial_\mu \varphi_x^\alpha \partial_\mu \varphi_x^\alpha + \frac{1}{2} m_0^2 \varphi_x^\alpha \varphi_x^\alpha + \frac{1}{4} \lambda_0 \left(\varphi_x^\alpha \varphi_x^\alpha \right)^2 \right] \tag{32}$$

10

and using $\partial_\mu \varphi_x^\alpha = \varphi_{x+\hat{\mu}}^\alpha - \varphi_x^\alpha$, we obtain

$$S = \sum_{x\mu} \varphi_x^\alpha \varphi_{x+\hat{\mu}}^\alpha - \sum_x \left[\frac{1}{2} \left(2d + m_0^2 \right) \varphi^2 + \frac{1}{4} \lambda_0 \left(\varphi^2 \right)^2 \right] \tag{33}$$

We now reparameterise the integral to facilitate a comparison with the XY model Hamiltonian,

$$\varphi^\alpha = \sqrt{2\kappa} \phi^\alpha, \quad m_0^2 = \frac{1 - 2\lambda}{\kappa} - 2d, \quad \lambda_0 = \frac{\lambda}{\kappa^2} \tag{34}$$

The discretised action is then,

$$S = 2\kappa \sum_{x\mu} \phi_x^\alpha \phi_{x+\hat{\mu}}^\alpha - \sum_x \left[\phi_x^\alpha \phi_x^\alpha + \lambda \left(\phi_x^\alpha \phi_x^\alpha - 1 \right)^2 \right] \tag{35}$$

where in two dimensions, the first term is equivalent to the XY nearest neighbour Hamiltonian. We can take this further by considering the partition function to be,

$$Z = \left(\prod_{x\alpha} \int_{-\infty}^\infty d\phi_x^\alpha \right) \exp S \equiv \int D\mu(\phi) \exp \left(2\kappa \sum_{x\mu} \phi_x \phi_{x+\hat{\mu}} \right) \tag{36}$$

$$D\mu(\phi) = \prod_x d\mu(\phi_x), \quad d\mu(\phi) = d^n\phi \exp \left[-\phi^2 - \lambda \left(\phi^2 - 1 \right)^2 \right] \tag{37}$$

This volume integral reduces to the volume of a S^n sphere in the limit of $\lambda \to \infty$,

$$\frac{\int d\mu(\phi) f(\phi)}{\int d\mu(\phi)} \to \frac{\int d\Omega_n f(\phi)}{\int d\Omega_n} \tag{38}$$

and in two dimensions is

$$\frac{\int d\mu(\phi) f(\phi)}{\int d\mu(\phi)} \to \frac{\int r \, dr \, d\theta \, f(\phi)}{\pi r^2} \tag{39}$$

11

3 Numerical Procedure

3.1 The Monte Carlo Algorithm

Monte Carlo simulations were employed in the study of the systems. In statistical physics, Markov chain Monte Carlo methods obtain approximate values for averages over statistical ensembles through random sampling. In cases such as that of the XY model, where the number of possible configurations is actually infinite, direct sampling and exact evaluation of the partition function and expected value integrals are impossible tasks. Monte Carlo simulations provide a finite number of representative configurations that can approximate the distribution/integral/expected values of observables [6].

A square lattice configuration of N x N spin states, represented by angles $\theta_{i,j} \in (0, 2\pi)$, $i, j \in (1, .., N)$, is randomly generated. Periodic boundary conditions are imposed on the finite volume system, such that

$$\vec{s}_{i,j} = \vec{s}_{i+N,j+N} \tag{40}$$

At each step of the Metropolis algorithm, a state in the configuration is chosen at random at which a new, trial state $\tilde{\theta}_{i,j}$ is randomly generated and accepted following a probability distribution proportional to the entropy of the system. If the trial state results in a lowering of the total energy of the system,

$$\Delta H = -J\left(\sum \cos\left(\tilde{\theta}_{i,j} - \theta_{i\pm1,j\pm1}\right) - \sum \cos(\theta_{i,j} - \theta_{i\pm1,j\pm1})\right) < 0 \tag{41}$$

where $\theta_{i\pm1,j\pm1}$ are the state's nearest neighbours in the two-dimensional lattice, the trial state is accepted. Otherwise is is accepted according to the probability distribution

$$P(S) = \frac{1}{Z} \exp\left(-\frac{1}{k_B T} H(S)\right) \tag{42}$$

where Z is the partition function of the ensemble

$$Z = \int DS \exp\left(-\frac{1}{k_B T} H(S)\right) \tag{43}$$

meaning that the trial state is accepted if a random number between 0 and 1 is less than

$$\frac{P(\tilde{S})}{P(S)} = \exp\left(-\frac{1}{k_B T}\Delta H\right) \tag{44}$$

where k_B, Boltzmann's constant and J, the coupling, have units 1 in our model. The temperature T of the configuration accordingly affects the acceptance probability of trial states.

The transition probability obeys the properties of positivity, symmetry and completeness,

$$P(S \to S') \geq 0, \quad \sum_{S'} P(S \to S') = 1, \quad P(S \to S') = P(S' \to S) \tag{45}$$

and is a Markov Chain; that is to say that the probability of each trial state $\tilde{\phi}i + 1$ depends only on the state attained in the previous event and is the same for all i.

The expected value of a physical observable in the continuum limit is

$$\langle O \rangle = \frac{1}{Z} \int D\phi \exp[S(\phi)] O(\phi) \tag{46}$$

The Monte Carlo method approximates these integrals as summations which approach the continuous limit for larger and larger number of updates K,

$$\langle O \rangle \approx \bar{O} \equiv \frac{1}{K} \sum_{i=1}^{K} O(\phi_j) \tag{47}$$

Repeating this process for sufficiently updates will eventually lead to the desired probability distribution. The process of reaching a satisfactory configuration is called equilibration and this equilibration time τ_{eq} varies depending on the observable in question as well as the

temperature and size of the configuration. It is essential that this state of thermodynamic equilibrium is reached before evaluating physical observables, and the computational expense of the increase in equilibration time for exploring larger volumes and smaller lattice spacings enforces limitations on the practicality of larger simulations.

3.2 XY Model

The partition function of a statistical ensemble of spins $\theta_{i,j}$ in the XY model is

$$Z = \int D\theta \exp\left[\frac{1}{T}\sum_{\langle l,k\rangle}\cos\left(\theta_l - \theta_k\right)\right] \tag{48}$$

with expected values of observable O,

$$\langle O\rangle = \frac{1}{Z}\int D\theta O(\theta)\exp\left[\frac{1}{T}\sum_{\langle l,k\rangle}\cos\left(\theta_l - \theta_k\right)\right] \tag{49}$$

where $< l, k >$ denote nearest neighbours in two dimensions. The Markov chain is implented by randomly generating a trial angle $\tilde{theta} \in (0, 2\pi)$ for each step and following this probability distribution. Lattice discretisation of the Monte Carlo approach taking equilibration time τ_{eq} into account is

$$\langle O\rangle_{\mathrm{MC}} = \frac{1}{\tau_{tot} - \tau_{eq}}\sum_{t_k=\tau_{eq}}^{\tau_{tot}} O_{t_k} \tag{50}$$

where O_{t_k} is the value of the observable evaluated on the $\tau_{k\mathrm{th}}$ configuration step.

The expected value of the mean energy per spin,

$$< E >= \frac{1}{\tau_{tot} - \tau_{eq}}\int_{\tau_{eq}}^{\tau_{tot}} E(t)dt \tag{51}$$

14

is given by,

$$< E >= -\frac{1}{\tau_{tot} - \tau_{eq}} \sum_{t_k=\tau_{eq}}^{\tau_{tot}} \frac{1}{4N^2} [\sum_{<i,j>} \cos\left(\theta_i\left(t_k\right) - \theta_j\left(t_k\right)\right)] \tag{52}$$

The specific heat capacity is determined from the energy either as a variance or as a derivative, where both approaches should quantitatively agree (and qualitatively by reintroducing k_B),

$$C_V = \frac{1}{k_B T^2} \left(< E^2 > - < E >^2\right) \qquad = \frac{\Delta E}{\Delta T} \tag{53}$$

The mean magnetisation of the system is similarly calculated,

$$M(t) = \frac{1}{N^2} \sum_i \left(\cos\theta_i(t), \sin\theta_i(t)\right) \tag{54}$$

$$< M >= \frac{1}{\tau_{tot} - \tau_{eq}} \sum_{t_k=\tau_{eq}}^{\tau_{tot}} \left[\frac{1}{N^2} \left(\sum_i \cos\theta_i\left(t_k\right), \sum_i \sin\theta_i\left(t_k\right)\right)\right] \tag{55}$$

The susceptibility of the system is analogously,

$$\chi = \frac{1}{k_B T^2} \left(< M^2 > - < M >^2\right) \qquad = \frac{\Delta M}{\Delta T} \tag{56}$$

The final observable we evaluate in this study is the correlation function. The correlation function between two spins located at $\vec{s}$ and $s \vec{\mp} r$ is defined as

$$C(\vec{s}, s \vec{\mp} r) = \langle \vec{S}(s) \cdot \vec{S}(s + r) \rangle \tag{57}$$

The XY model is translation invariant due to its periodic boundary conditions and so the

correlation function only depends on the distance between the spins,

$$C(r) = <\cos(\theta_i - \theta_j)> \tag{58}$$

$$= \cos\theta_i \cos\theta_j + \sin\theta_i \sin\theta_j \tag{59}$$

with $r_{ij} = \vec{r_i} - \vec{r_j}$ the radius between states in the configuration.

For large system sizes, this can be a taxing and noisy computation and so a plane correlation function approximation is used whereby the correlation function is reduced to computing the average spin between planes,

$$C(d_{ab}) = <\cos\theta>_a <\cos\theta>_b + <\sin\theta>_a <\sin\theta>_b \tag{60}$$

with d_{ab} the distance between planes in the configuration.

3.3 O(2) Model

The discretised action of an O(n) field theory, as discussed in chapter 2, is

$$S = 2\kappa \sum_{x\mu} \phi_x^\alpha \phi_{x+\hat{\mu}}^\alpha - \sum_x \left[\phi_x^\alpha \phi_x^\alpha + \lambda \left(\phi_x^\alpha \phi_x^\alpha - 1 \right)^2 \right] \tag{61}$$

A two-dimensional field in two dimensions can be written in the form

$$\phi_x = \begin{bmatrix} r_x \cos\theta_x \\ r_x \sin\theta_x \end{bmatrix} \tag{62}$$

which reduces the action to

$$S = 2\kappa \sum_{x\mu} r_x r_{x\pm\mu} \cos(\theta_x - \theta_{x\pm\mu}) - \sum_x \left[r_x^2 + \lambda \left(r_x^2 - 1 \right)^2 \right] \tag{63}$$

16

for parameters κ and λ. The partition function is then

$$Z = \left(\prod_{x\alpha} \int_{-\infty}^{\infty} d\phi_x^{\alpha}\right) \exp S \equiv \int D\mu(\phi) \exp\left(2\kappa \sum_{x\mu} \phi_x \phi_{x+\hat{\mu}}\right) \tag{64}$$

and the Markov chain is implemented following this probability distribution, where the action S is equivalent to the Hamiltonian H in the spin case. Now however the trial fields are generating by deviating only marginally from the existing field, $\phi_x^{\alpha} \pm \delta$ The magnetisation of the field configuration per field is then just the average field value,

$$\langle \phi^{\alpha} \rangle = \sum_{x} \frac{\phi_x^{\alpha}}{N^2} \tag{65}$$

and the energy of the field configuration per field is the equivalent to the action

$$\langle E \rangle = -\frac{S}{N^2} \tag{66}$$

The correlation function $G_{xy}^{\alpha\beta}$ is

$$G_{xy}^{\alpha\beta} = \langle \phi_x^{\alpha} \phi_y^{\beta} \rangle - \langle \phi_x^{\alpha} \rangle \langle \phi_y^{\beta} \rangle \tag{67}$$

In the $\lambda \to \infty$ limit the field configuration favours a uniform radial distribution, $\langle r \rangle = 1$ and the energy reduces to the nearest neighbour interaction

$$\lim_{\lambda \to \infty} E \to \frac{1}{4N^2} \sum_{x\mu} \phi_x^{\alpha} \phi_{x+\hat{\mu}}^{\alpha} \tag{68}$$

3.4   Error Analysis

If each configuration in the Monte Carlo algorithm were independent, the statistical error of a variable O would be calculated in a straight forward manner from the variance σ_O^2 of the

dataset,

$$\delta O = \sqrt{\frac{\sigma_O^2}{n}} \tag{69}$$

where

$$\sigma_O^2 = \langle O \rangle_{MC}^2 - \langle O^2 \rangle_{MC} \tag{70}$$

In our case however, two subsequent configurations are correlated and our analysis of the statistical error becomes more involved.

3.4.1   Autocorrelation Time

The autocorrelation function is defined as,

$$\Gamma_O(t) = \langle O_k O_{k+t} \rangle - \langle O \rangle^2 \tag{71}$$

or more explicitly,

$$\Gamma_O(t) = \frac{1}{\tau_{tot} - \tau_{eq} - t} \sum_{k=\tau_{eq}}^{\tau_{tot}-t-1} O_{k+t} \left(O_i - \frac{1}{\tau_{tot} - \tau_{eq} - t} \sum_{j=\tau_{eq}}^{\tau_{tot}-t-1} O_j \right) \tag{72}$$

The autocorrelation function decays exponentially for large t,

$$\Gamma_O(t) \propto \exp\left(-\frac{t}{\tau_{auto}} \right) \tag{73}$$

and the autocorrelation time τ_{auto} can be used to calculate the correlated statistical error,

$$\delta O = \sqrt{\frac{2\tau_{\text{int},O}\sigma_O^2}{n}} \tag{74}$$

where the integrated autocorrelation time $\tau_{\text{int},O}$ is the series of contributions,

$$\tau_{\text{int},O} = \frac{1}{2} + \sum_{t=1}^{+\infty} \frac{\Gamma_O(t)}{\sigma_O^2} \tag{75}$$

which is truncated when the errors of the remaining terms outweigh their contributions.

It can be difficult to determine the exact step at which the integrated autocorrelation time should be truncated and it is worth considering a secondary method of error analysis.

3.4.2 Binning

Divide the data set into N_B bins of size B, where B is much larger than the autocorrelation time τ_{auto}. The bins can then be thought of as independent configurations (they are still correlated at their boundaries but these effects can be neglected) and the error of the average $\langle O \rangle_{N_B}$ of the bins can be calculated as in Eq().

It is worth noting here that some idea of the autocorrelation time for each variable must still be known to ensure an accurate adoption of this method. Binning also requires larger amounts of data.

4 Results and Discussion

4.1 XY Model

The Monte Carlo algorithm was used to compute the observables of the XY spin model in systems of lattice size 20x20, 40x40 and 80x80.

4.1.1 Spin Configuration

The configuration of spins at thermodynamic equilibrium of temperatures in the low and high temperature regimes are shown in Figure 7. The spins are aligned in Figure 7a and are disordered in Figure 7b. Figure 8 shows the remnants of vortices and anti-vortices in
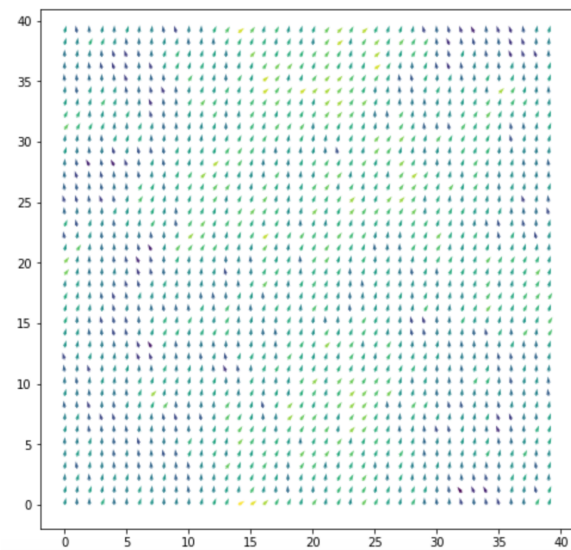
(a) Low temperature regime.
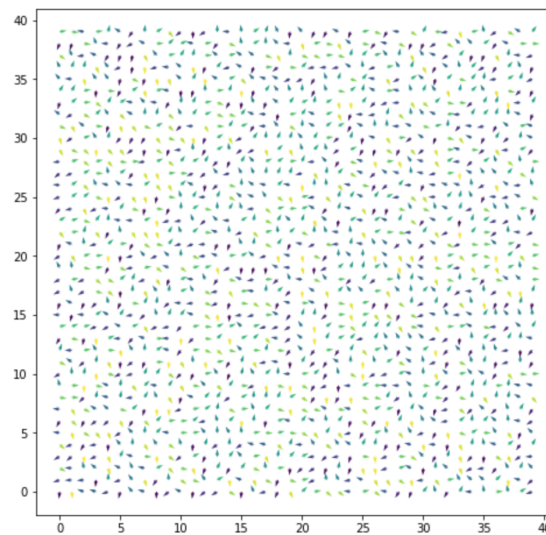
(b) High temperature regime.

Figure 7: Spin configuration.

the critical temperature regime. These bind together below this temperature producing the symmetric, aligned phase in Figure 7a.
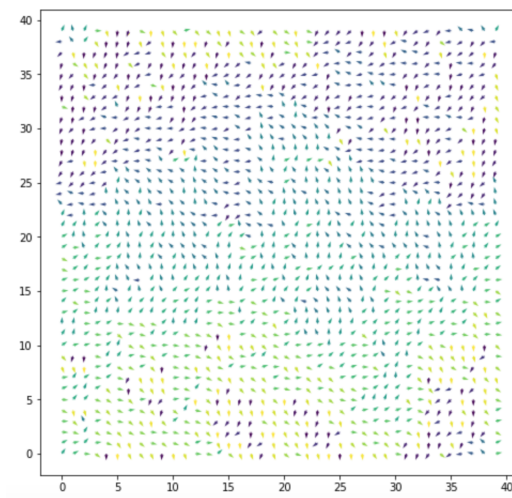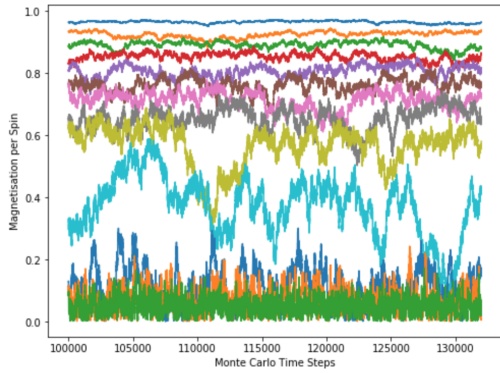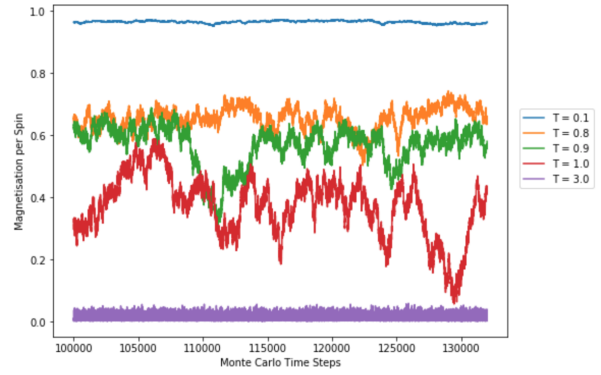

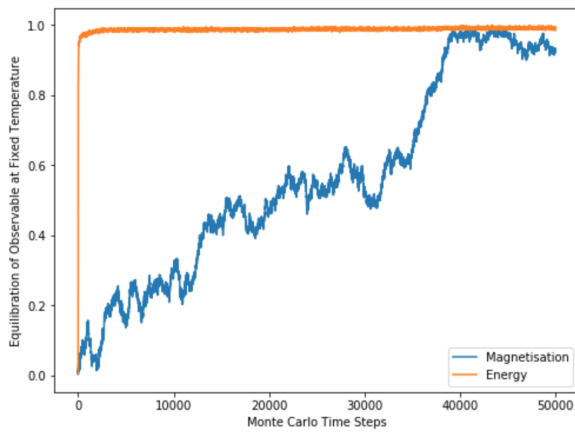Figure 8: Spin configuration at critical temperature.
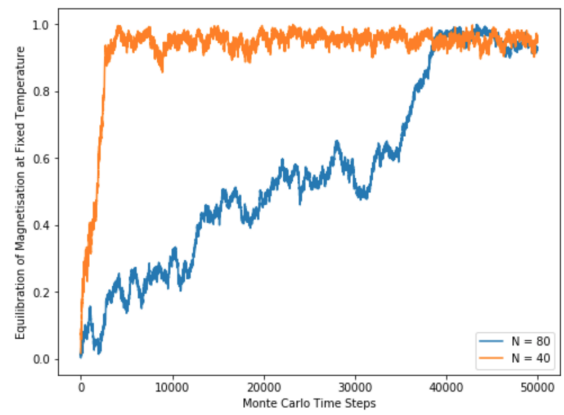
(a) All temperatures

(b) Low, critical and high temperature regimes

Figure 9: Equilibrated Magnetism with Time

(a) Equilibration time with observable.

(b) Equilibration time with lattice size N.

Figure 10: Equilibration Times.

21

4.1.2 Equilibration

The observables were monitored with time to ensure thermodynamic equilibrium was reached before determining their mean values. Figure 9 shows the equilibration times of magnetism for various temperatures. Equilibration time was faster in the high temperature regime in comparison with the low temperature regime due to an intrinsically higher acceptance frequency in the Metropolis algorithm. The notion of "equilibrium" becomes less clear in the highly fluctuating region of the critical temperature, as shown in the mid range temperatures in Figure 9b. This behaviour highlights the phase change between the symmetric and Kosterlitz-Thouless phases of the model.

Figure 10 shows the relative time taken to reach thermodynamic equilibrium for various observables and lattice sizes. Energy equilibrates much faster than magnetism, and the equilibration time $2N^2$, making it computationally more intensive to simulate larger lattice sizes, though larger lattice sizes more accurately represent the infinite volume case. There is therefore a computational trade off and it was found that generally the $N = 40$ case gave the most reliable results.

4.1.3 Energy

The normalised mean energy and heat capacity per spin of the equilibrated system is shown in Figure 11. The two different methods for calculating the heat capacity produced analagous results and so only the derivative approach is shown in the figure.

The heat capacity begins to sharply increase at $T = 0.9$ and peaks at $T = 1.1$ before decaying to zero for high temperature. This shows a phase transition at $T = 0.9$ at which the energy of the system increases suddenly and levels off for high temperature. This is consistent with the unbinding of vortex-antivortex pairs at the critical temperature which increases the total entropy of the system.
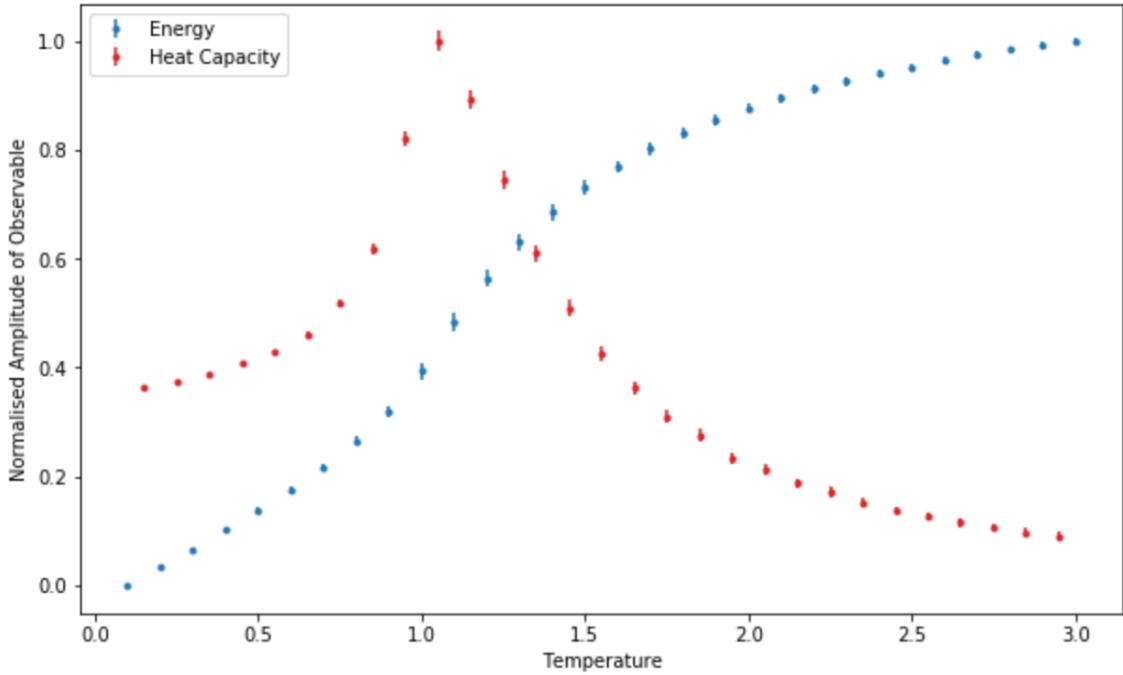
Figure 11: Energy and Heat Capacity with Temperature.

4.1.4 Magnetism

The normalised mean magnetism and susceptibility per spin of the equilibrated system is shown in Figure 12. As in the case of energy, the two different methods for calculating the susceptibility produced analagous results and so only the derivative approach is shown in the figure. The magnetism of the system at low temperature is at its maximum due to the highly aligned nature of the spin configuration in Figure 7a. The susceptibility also begins to sharply increase at $T = 0.9$ and peaks at $T = 1.1$ before decaying to zero for high temperature. This shows a phase transition at $T = 0.9$ at which the magnetism of the system decreases suddenly and decays to zero. This is consistent with the disordered configuration in Figure 7b. The proliferation of vortex-antivortex pairs at the critical temperature has no effect on the long-range order of the system.
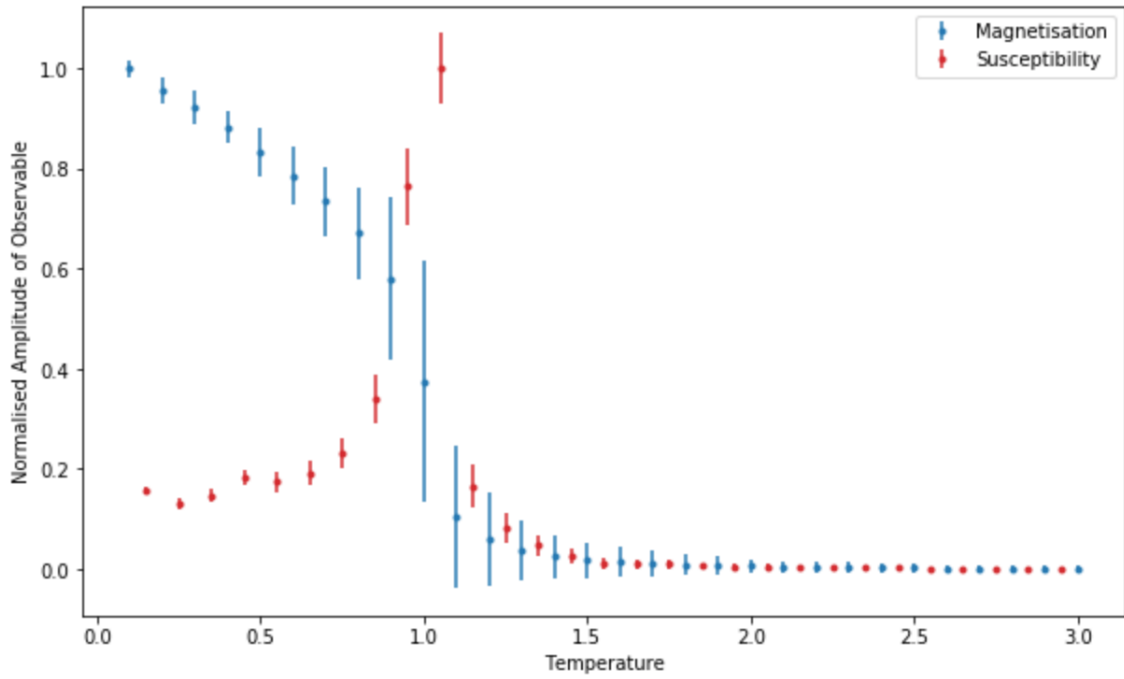
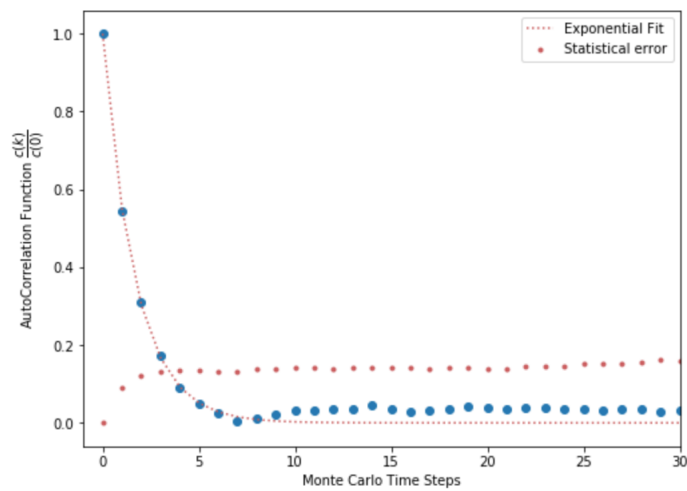Figure 12: Magnetism and Susceptibility with Temperature.

Figure 13: Estimate of the Autocorrelation Time using the Autocorrelation Function Best Fit and Statistical Error.
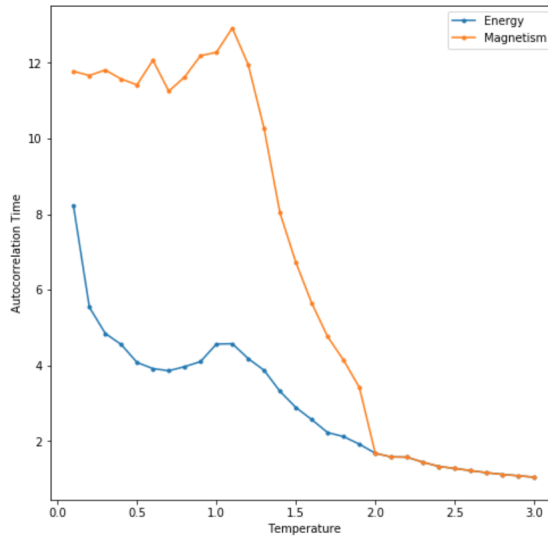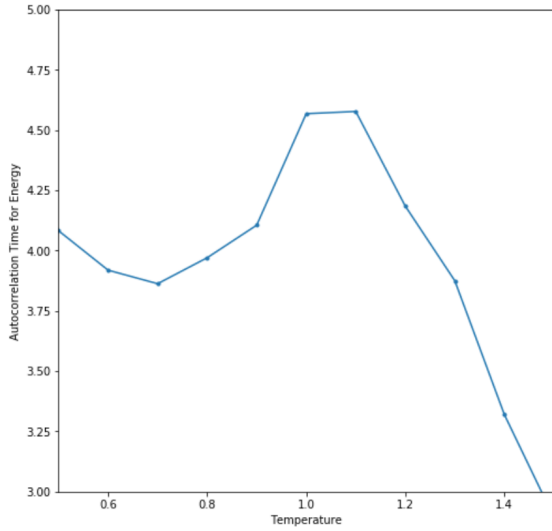
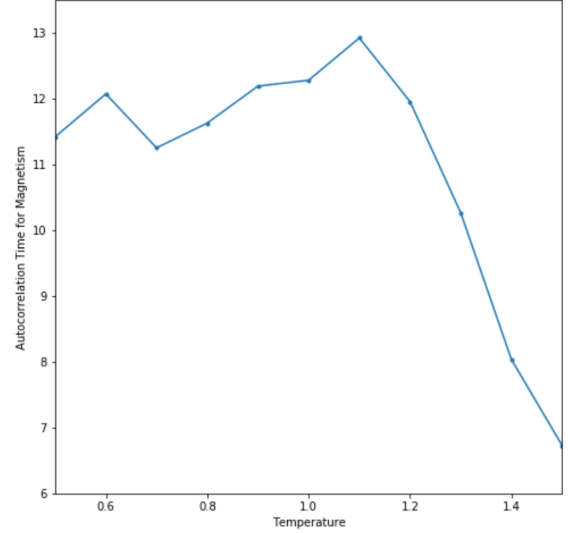Figure 14: Autocorrelation Times with Temperature.

4.1.5 Error Analysis

Errors shown were calculated using autocorrelation time estimates. The method of estimation is illustrated in Figure 13, where the sum of the autocorrelation terms is trunctated when the statistical error of the data point is larger than the data point itself - when the contribution is deemed more noisy than useful.

Autocorrelation times for energy and magnetism are shown in Figure 14. Magnetic autocorrelation time was greater than that of energy, which was expected given the larger equilibrium time. Autocorrelation times were longer in the low temperature regime than in the high. This stronger correlation between configurations at very low temperatures made it more computationally-intensive to estimate observables accurately, and a compromise between reasonable simulation times and low temperature estimates must be considered. This stronger correlation however also highlights the aligned spin configuration in this phase. The autocorrelation time appears to gradually decrease with increasing temperature until its phase transition where it peaks and then decays to a minimum at high temperature, showing the uncorrelated behaviour of high temperature spin configurations.

(a) Energy

(b) Magnetism

Figure 15: Autocorrelation Times around the Critical Temperature.

The autocorrelation time decreases slowly with temperature as shown in Figure 15 until it begins to increase at $0.8T$ with a local maximum again at $T = 1.1 - 1.2$, before decaying rapidly to a minimal value of $\tau_{auto} = 1$, showing the data points are uncorrelated at high temperature. This is consistent with a critical temperature at $T = 0.8$.

The binning method was used to verify the autocorrelation error analysis of lower sized lattices but was too computationally intensive to carry out for $N = 80$.

4.1.6 Correlation Function

Figure 16 shows the correlation functions for various temperatures calculated for the largest lattice size $N = 80$. Spins are completely correlated at $T = 0.1$ and rapidly decay to zero in the high temperature regime. Errors for correlation functions in the critical region of $T = 0.8 - 1$ are significantly larger than elsewhere due to the highly fluctuating nature of the spins at this point, consistent with a phase transition.

Figure 17 shows the optimised best radial decay fit for correlation lengths. The radial decay is in the low temperature regime (Figure 17a) a suitable fit but above the critical
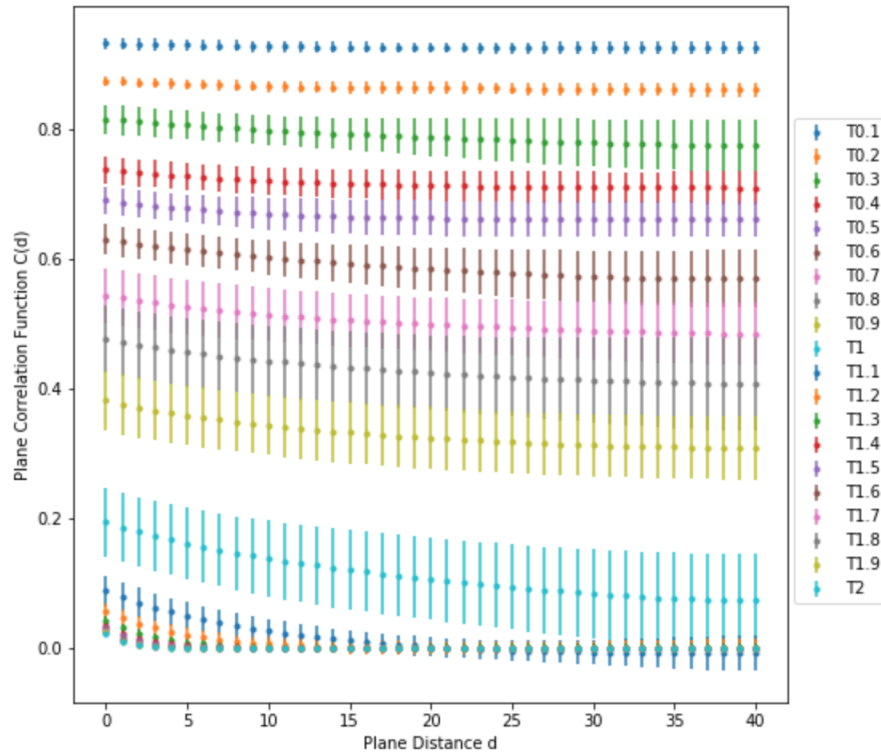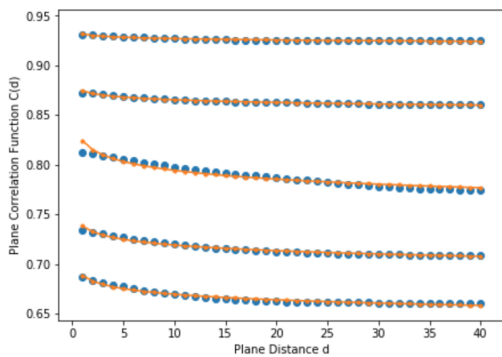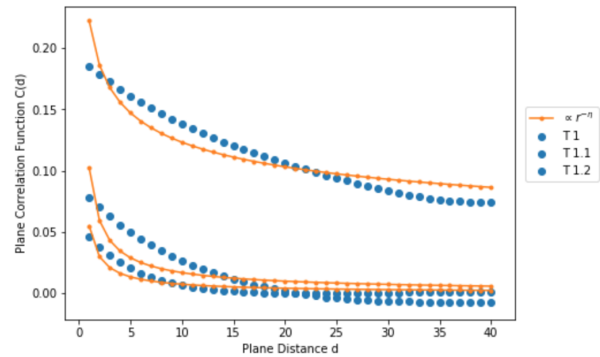
26

Figure 16: Correlation Functions with Temperature.

(a) Low Temperature Regime.

(b) High Temperature Regime.

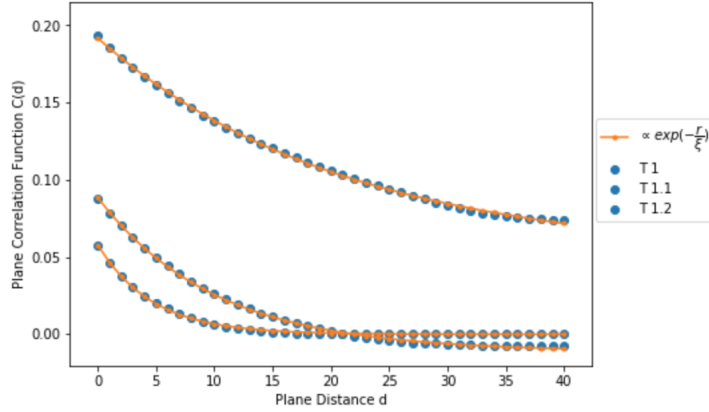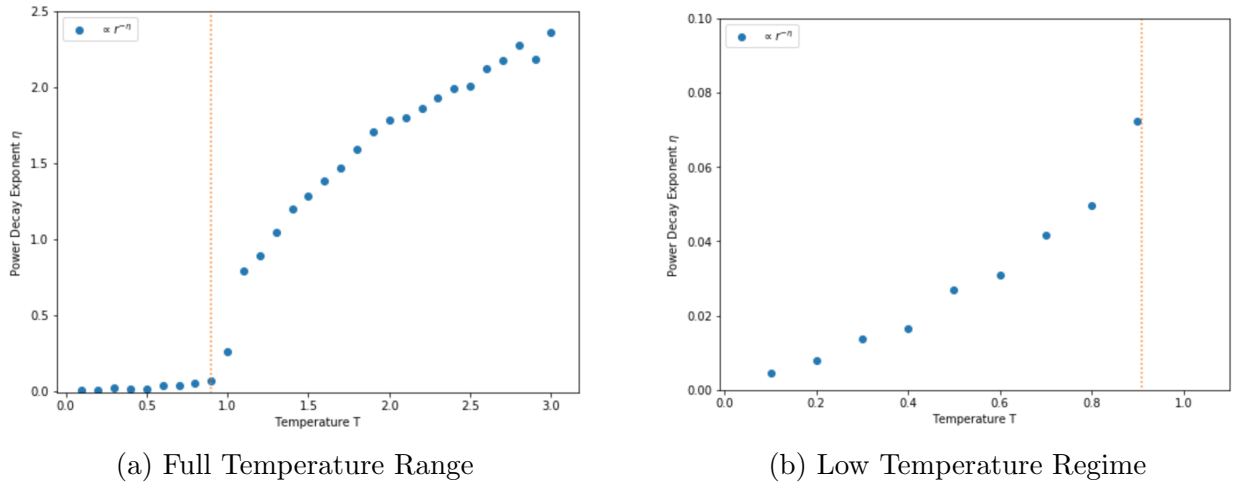Figure 17: Radial Decay Fit of Correlation Functions

Figure 18: Exponential Fit of Correlation Functions in the High Temperature Regime.


(a) Full Temperature Range


(b) Low Temperature Regime

Figure 19: Radial Decay Fit of Correlation Functions.

temperature begins to deviate significantly from the data (Figure 17b). An exponential fit of the high temperature data is contrastingly shown in Figure 18 and indicates a clear change in the correlation function behaviour around the critical point which is consistent with the Kosterlitz-Thouless phase transition.

Figure 19a shows the best fit radial decay exponent η across the full temperature range. There is a sudden significant increase at $T = 0.9$ at which we know from 19 that above this temperature the power fit ceases to be an accurate fit of the data. Figure 19b then shows the exponent values of interest. The exponent increases linerealy with temperature in
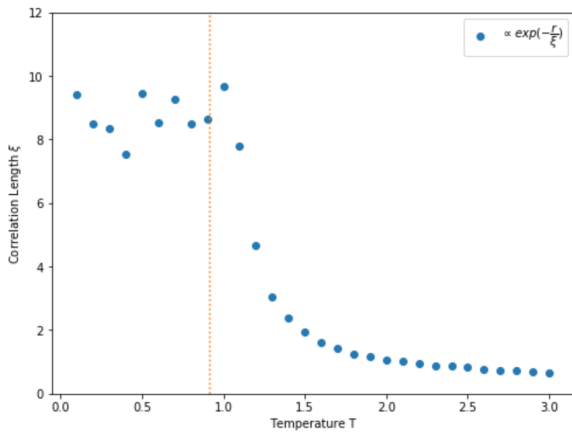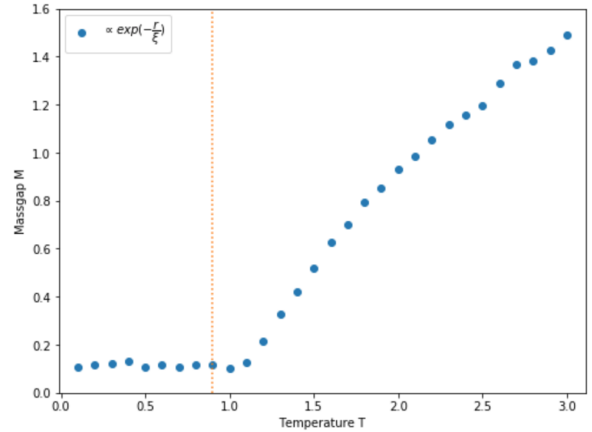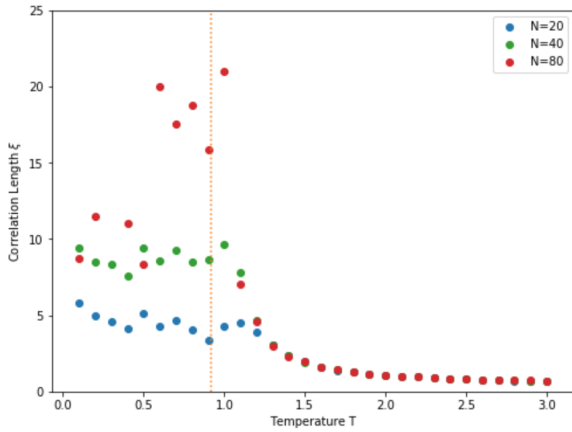
(a) Correlation Length　　　　　　　　(b) Mass Gap

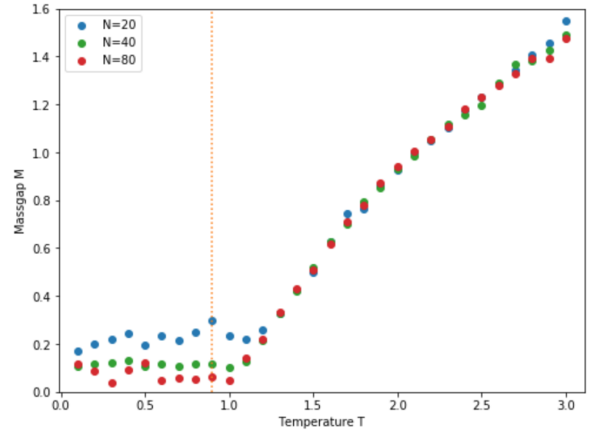Figure 20: Correlation Length and corresponding Mass Gap of the XY model for N=40.

the symmetric phase, tending towards a maximum oof $\eta \approx 0.08$ at the critical temperature, which is consistent with current literature values of $\eta \approx 0.1$. The slow radial decay of the system below $T = 0.9$ but not above it indicate the presence of a phase transitionas predicted by Kosterlitz and Thouless.

Figure 20a shows the best fit correlation length ξ across the full temperature range for $N = 40$ lattice sizes and Figure 21b shows the corresponding mass gaps M. In the high temperature phase approaching the critical temperature, the correlation length asymptotically grows from zero to a finite maximum of $xi = 10$. It remains at this maximum in the symmetric phase of the system. The mass gap accordingly decreases from a maximum as it approaches the critical temperature from above, stabilising at $M = 0.1$ at $T = 1.0$.

If various lattice sizes were not considered, 20 would lead one to believe there is a finite correlation length and finite massgap at the critical temperature, implying the occurence of spontaneous symmetry breaking with the creation of a massive Golstone boson. This would violate the Mermin Wagner Theorem and contradict Kosterlitz Thouless theory. Figure **??** however shows evidence of a lattice artefact in the correlation length. The correlation length is invariant across lattice sizes in the high temperature regime but the local maximum at the

(a) Correlation Length   (b) Mass Gap

Figure 21: Correlation Length and corresponding Mass Gap of the XY model for different lattice size N.

critical temperature is proportional to the size of the system, with maxima $xi = 20, 10, 5$ for lattice sizes $N = 80, 40, 20$. Thus the correlation length asymptotically grows with a limit that is proportional to the size of the system. We can extrapolate that there is a divergent correlation length at the critical temperature, as predicted by the Kosterlitz-Thouless. Figure **??**(a) analagously shows the mass gap tending towards some constant inversely proportional to lattice size in the low temperature phase, i.e. the mass gap tends to zero for infinite volume. This is again consistent with the Kosterlitz-Thouless phase transition.

The vacuum expectation value is shown in Figure 22. The value sharply rises from zero at the critical temperature to a a maximum. This result is not as useful in highlighting the absence of spontaneous symmetry breaking, as we would expect the maximum to decrease as the lattice size increased. The values do slightly decrease but it is likely that the lattice sizes were too small in this case to accurately represent the infinite volume model.

4.1.7 Ising Model

To emphasise the effect of symmetry on statistical spin models, analagous calculations were carried out on the two-dimensional Ising model. The system has a discrete symmetry rather
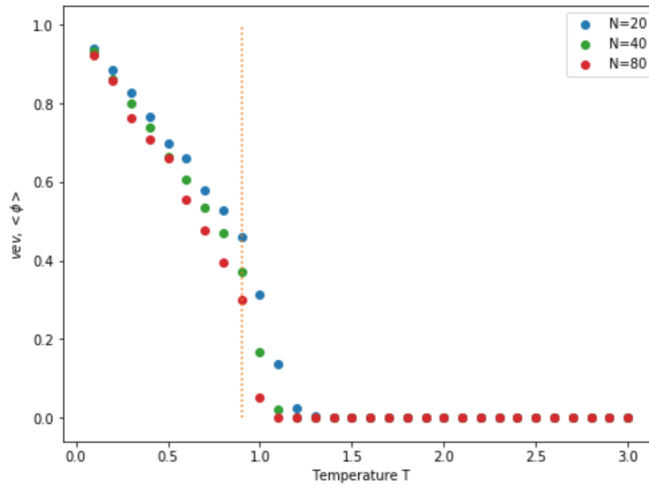
Figure 22: Vacuum expectation value of the XY model for different lattice size N.

than a continuous symmetry in the case of the XY model, and so is not in violation of the Mermin-Wagner Theorem. Accordingly spontaneous symmetry breaking is not forbidden. Figure 23 shows the correlation length
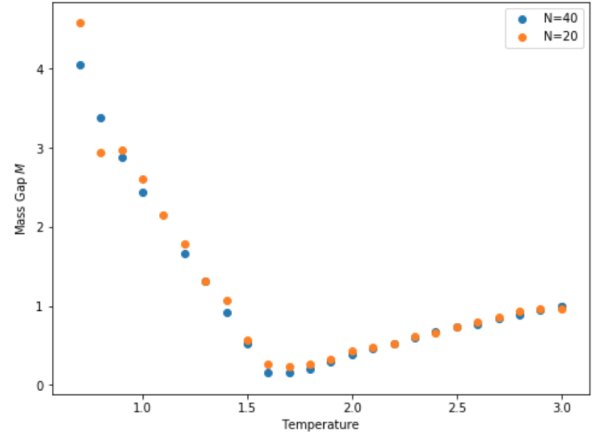
xi and corresponding mass gap M of the Ising model for lattice sizes $N = 20, 40$. The critical temperature of this system is higher, at a temperature of $T \approx 1.5 - 1.6$. Figure 23a shows a peak in

xi at the critical temperature that again appears to scale with system volume. The asymptotic increase in the high temperature regime is similar to that of the XY model but the rapid decay in the low temperature regime is in stark contrast to the XY model. Indeed, in Figure 23b, while the massgap of the XY model tends to zero in the symmetric phase, it contrastingly tends to a non-zero constant in the case of the Ising model, regardless of the size of the system. This highlights the unique nature of the phase transition in the case of the XY model and its distinction from spontaneous symmetry breaking. This discrete symmetry system is permitted to produce a massive excitation but the continuous nature of the XY model enforces a massless phase transition.

The vacuum expectation value of the Ising model is shown in Figure 24. The value
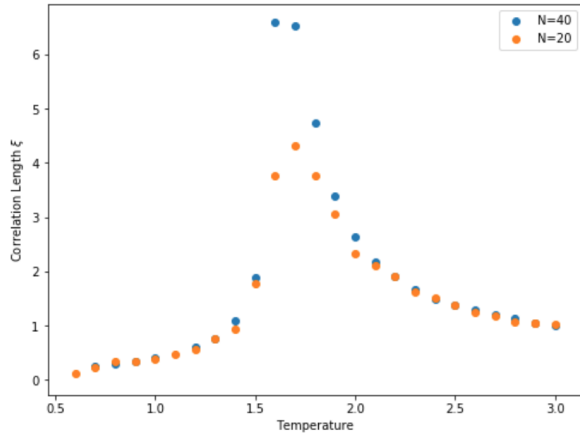
(a) Correlation Length

(b) Mass Gap

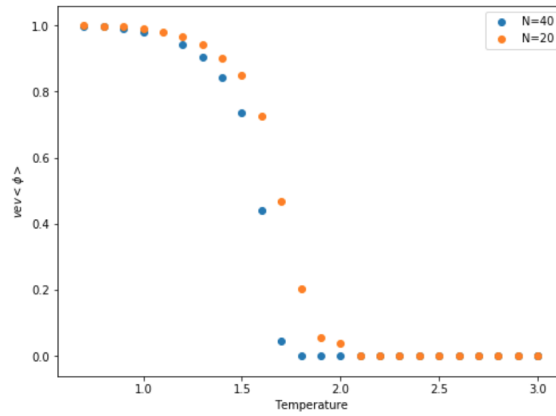Figure 23: Correlation Length and corresponding Mass Gap of the Ising model for different lattice size N.

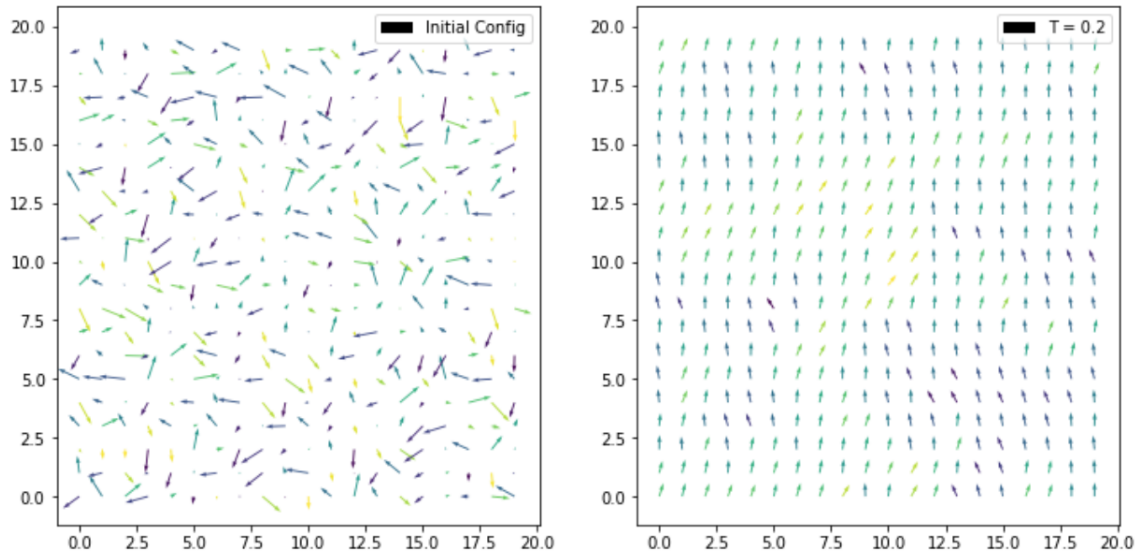Figure 24: Vacuum expectation value of the Ising model for different lattice size N.

Figure 25: Spin configuration of the O(2) model at low temperature in the $\lambda \to \infty$ limit.

sharply rises from zero at the critical temperature to a constant in the symmetric phase regardless of lattice size. The behaviour fits that of a step function that is not exhibited in the XY model.

4.2 Field Theory Model

The Monte Carlo algorithm was adapted to compute the observables of the O(2) model in systems of lattice size 10x10. Computational effort was much higher in this model due to the extra parameter in the field configuration resulting in much longer equilibration times. The acceptance frequency was lower than in previous cases and was difficult to keep at a reasonable level for higher λ, making it verification of the model's equivalence to the XY model difficult.

The configuration of spins at thermodynamic equilibrium of temperatures in the low and high temperature regimes are shown in Figure ?? for $\lambda >> 1$. The spins are aligned in Figure 25 and are disordered in Figure 26. The probability distribution determined by the discretised path integral favoured field configurations with spin amplitude $r = 1$, as shown in
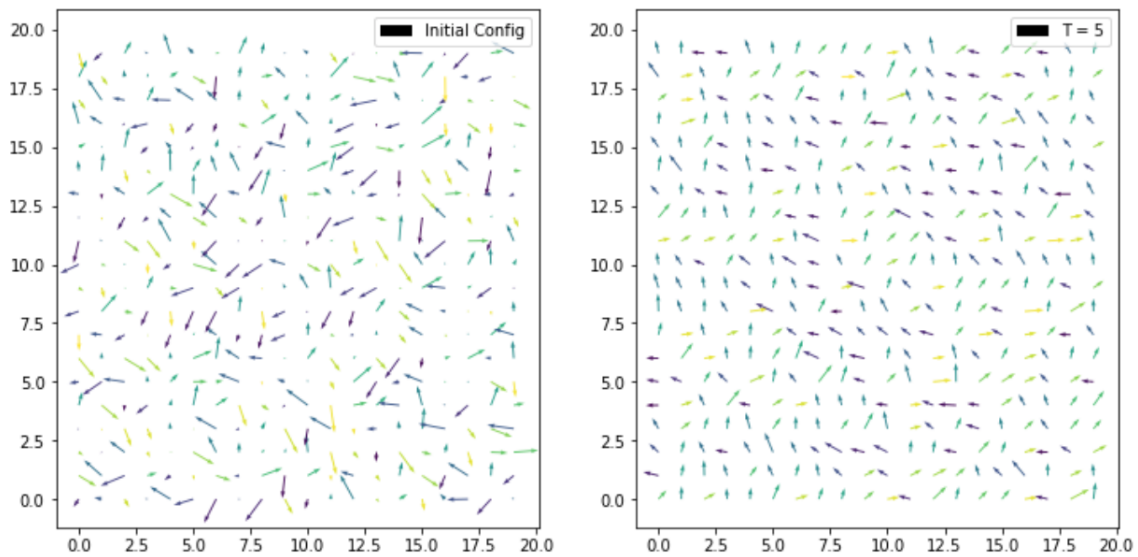
Figure 26: Spin configuration of the O(2) model at high temperature in the $\lambda \to \infty$ limit.

the figures. As such, even with the extra spin parameter, the configurations match that of the XY model.

Figure 27 shows the remnants of vortices and anti-vortices in the critical temperature regime. These bind together below this temperature producing the symmetric, aligned phase in Figure 7a.

Figure 28 shows a crude estimation of the magnetism of the spin configuration in the O(2) model. Larger lattice sizes and longer simulation times are required to give quantitative results but these provisional results show a general agreement with the comprehensive XY model, with a maximum magnetic alignment at low temperature and sharply beginning to decrease to zero around the critical temperature. The susceptibility was not sufficiently equilibrated to include here.
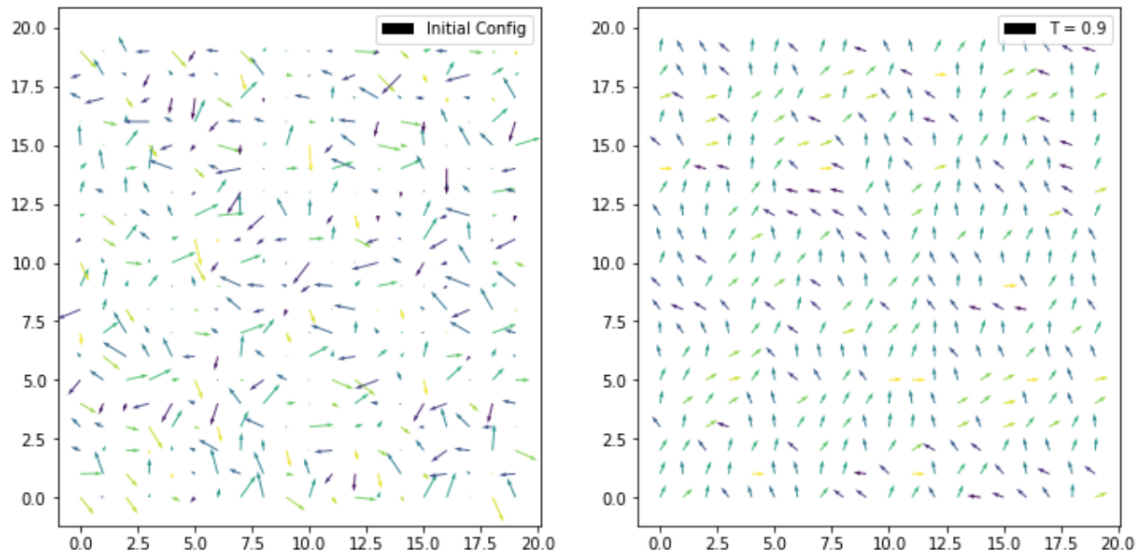
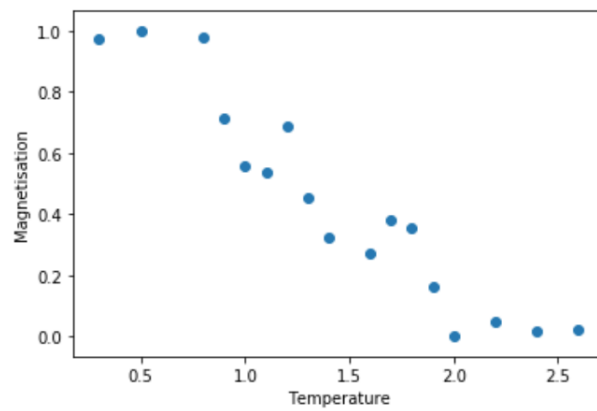Figure 27: Spin configuration of the O(2) model at the critical temperature in the $\lambda \to \infty$ limit.

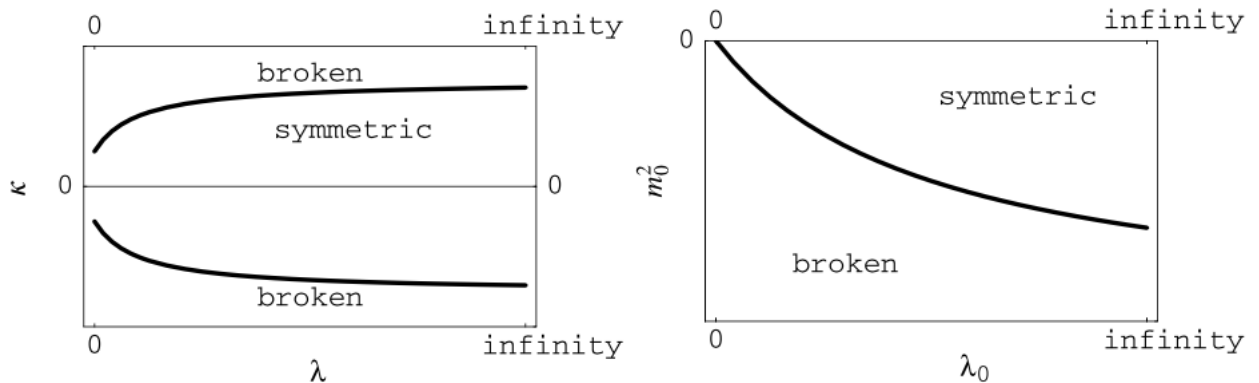Figure 28: Magnetism of the O(2) model with Temperature.

Figure 29: Critical lines in the $\kappa - \lambda$ plane and the $m_0^2 - \lambda_0$ plane (qualitative)**??**.

5   Future Research

Emphasis in this project was on the qualitative and quantitative success and limitations of a numerical Monte Carlo algorithm in simulating the XY model and extension of the algorithm to describe an O(2) field theory. There are many possibilities for deeper research into the behaviour of the field theory. The field theory model was shown to qualitatively converge to describe the physics of the XY model at $\lambda \to \infty$ but the full $\kappa - \lambda$ phase diagram was not studied in detail. Future research would expand this study by simulating the field model at varying λ to determine how κ_{crit} across the entire parameter space, as shown in Figure 29.

6   Conclusions

Overall the numerical simulations were an accurate representation of the classical XY model. It can be satisfactorily concluded from the above comparison that the phase transition in the XY model is distinct from that of spontaneous symmetry breaking and is rather a topological phase transition from bound to unbound vortices. The field theory simulations gave qualitatively analogous results to the XY spin model at infinite λ, showing an underlying mathematical equivalence between the quantum and spin systems, but the Monte Carlo techniques required for a comprehensive analysis of the field model were too time and computation

intensive for the breadth of this project and further research is necessary to gain a qualitative understanding of how the O(2) field model behaves.

References

[1] Lygouras, C., Topological vortices in the XY model at low temperatures. *https://commons.wikimedia.org/* 2020

[2] Kosterlitz, J. M. , Thouless, D. J. , Ordering metastability and phase transitions in two-dimensional systems. *J. Phys. C: Solid State Phys*, 6 1181, 1973

[3] Tolley, A. , Advanced Quantum Field Theory. *Imperial College London*, 2021

[4] Rajantie, A. , Unification. *Imperial College London*, 2021

[5] Smit, J. , Introduction to Quantum Fields on a Lattic.e *Cambridge University Press*, 2002

[6] Gupta, R. , Baillje, C. , Critical behavior of the two-dimensional XY model. *Physical Review*, Volume 45, Number 6 1992

[7] Mermin, N.D., Wagner, H., Absence of Ferromagnetism or Antiferromagnetism in One- or Two-Dimensional Isotropic Heisenberg Models. *Phys. Rev. Lett.*, 17 (22): 1133–1136. 1966

[8] Kosterlitz, J. M., The critical properties of the two-dimensional xy model. *J. Phys. C: Solid State Phys.*, 7 1046, 1974

[9] Jensen, H. J., The Kosterlitz-Thouless Transition. *https://www.mit.edu/ levitov/8.334/notes/XYnotes1.pdf.* 2020

[10] Onsanger, L., Crystal Statistics. I.A Two-Dimensional Model with an Order-Disorder Transition. *Physical Review*, Volume 65, Number 3. 1944

[11] Spitzer, F., Principles of Random Walk. *Princeton:Van Nostran* pp 148-51. 1964